

## Rapid Establishment of Chemical and Mechanical Properties during Lamellar Bone Formation

B. Busa,<sup>1</sup> L. M. Miller,<sup>2</sup> C. T. Rubin,<sup>1</sup> Y.-X. Qin,<sup>1</sup> S. Judex<sup>1</sup>

<sup>1</sup>Department of Biomedical Engineering, State University of New York at Stony Brook, Stony Brook, NY, USA

<sup>2</sup>National Synchrotron Light Source, Brookhaven National Laboratory, Upton, NY, USA

Received: 16 August 2005 / Accepted: 22 August 2005 / Online publication: 5 December 2005

**Abstract.** The development of prophylaxes and treatments of bone diseases that can effectively increase the strength of bone as a structure necessitates a better understanding of the time course by which chemical properties define the stiffness of the material during primary and secondary mineralization. It was hypothesized that these processes would be relatively slow in the actively growing skeleton. Seven-week-old Sprague-Dawley female rats ( $n = 8$ ) were injected with multiple fluorochrome labels over a time span of 3 weeks and killed. Chemical and mechanical properties of the tibial mid-diaphysis were spatially characterized between the endocortical and periosteal surface by *in situ* infrared microspectroscopy and nanoindentation. The phosphate-to-protein ratio of bone 2–6 days old was 20% smaller at the periosteal surface and 22% smaller at the endocortical surface ( $P < 0.05$  each) compared to older intracortical regions. The ratios of carbonate to protein, crystallinity, type A/type B carbonate, collagen cross-linking, and bone elastic modulus did not differ significantly between bone 2–6, 10–14, and 8–22 days old and intracortical regions. Intracortical properties of 10-week-old rats, except for the carbonate-to-protein ratio which was 23% smaller ( $P < 0.01$ ), were not significantly different from intracortical matrix properties of young adult rats (5 months,  $n = 4$ ). Spatially, the phosphate-to-protein ratio ( $R^2 = 0.33$ ) and the phosphate-to-carbonate ratio ( $R^2 = 0.55$ ) were significantly correlated with bone material stiffness, while the combination of all chemical parameters raised the  $R^2$  value to 0.83. These data indicate that lamellar bone has the ability to quickly establish its mechanical and chemical tissue properties during primary and secondary mineralization even when the skeleton experiences rapid growth.

**Key words:** Cortical bone — Modeling — Growth — Nanoindentation — Infrared spectroscopy — Rat

Addition of tissue to surfaces of the skeleton, as modulated by complex interactions between genetic, molecular, and cellular factors, is integral to the processes of growth and development, adaptation to external and internal stimuli, as well as aging [1–3]. The mineralization of the

organic matrix secreted by osteoblasts occurs in two phases. Primary mineralization, as visualized by mineralizing fronts using histomorphometric techniques, involves the immediate addition of inorganic components to the matrix, while secondary mineralization focuses on increasing the number of mineral crystals and their degree of maturation and perfection. The time course of mineralization almost certainly depends on age and physiological status of the individual, but it is often assumed that primary mineralization takes a few days to several months and that secondary mineralization can take up to several years to attain peak levels [4–6]. Consistent with this view, turnover in a given bone is inversely related to its degree of mineralization [7].

Primary mineralization on surfaces may alter bone morphology and enhance its strength by the sheer addition of tissue, but for this to occur, it is clear that the newly added material has to be of high quality [8]. Bone quality is substantially influenced by morphological, cellular, and molecular variables but perhaps most strongly affected by microscopic chemical and mechanical material properties [9, 10]. Bone's organic and inorganic phases define its chemical and mechanical properties, but precise relationships and interactions between individual chemical and mechanical variables are, to a large degree, unknown. A large number of studies have related the strength and stiffness of bone to its mineral content [11–14], but clearly, other chemical properties pertaining to both the organic and inorganic phases also contribute to bone's mechanical properties. Crystal size, orientation, maturation, and perfection have been suggested to influence mechanical behavior [15, 16]. Changes in carbonate content and, in particular, carbonate substitution for phosphate ions alter crystal shape and the arrangement of the crystal lattice, leading to altered mechanical properties [15, 17]. Collagen provides tensile strength, toughness, resilience to fracture, and ductility; and the strength of collagen-mineral bonding and the quality, maturity, and orientation of the collagen fibers have been implicated in bone's mechanical behavior [18–23].

Correspondence to: S. Judex; E-mail: stefan.judex@sunysb.edu

During phases of early growth and development, bone gradually increases its mass and physical properties, including parameters of bone strength, at the level of the organ [18, 24]; but it is unclear how quickly new tissue added to bone surfaces during growth (modeling) matches the chemical and mechanical properties of much older bone found intracortically. Considering that accumulation of mineral to bone as an organ is incremental during skeletal growth [24, 25] and that mineral resources for both primary and secondary mineralization may be limited because of the high prevalence of surface modeling throughout the skeleton, we hypothesized that primary mineralization of lamellar bone during modeling would provide only a fraction of its intracortical properties and that secondary mineralization would be gradual and slow. Further, we hypothesized that the mineral content of the matrix would predominantly determine its micromechanical stiffness.

## Materials and Methods

### Experimental Design

All procedures were reviewed and approved by the university's Animal Care and Use Committee and met or exceeded all Association for Assessment & Accreditation of Lab Animal Care (AALAC) guidelines. Over a 3-week time span, female 7-week-old Sprague-Dawley rats ( $n = 8$ ) were injected intraperitoneally with multiple fluorochrome labels that were incorporated into actively mineralizing surfaces at the time of injection: calcein (15 mg/kg) was injected on days 1, 5, 17, and 21 and xylenol orange (90 mg/kg) was injected on days 9 and 13 (Fig. 1). Rats were killed on day 23 (10 weeks of age) and weighed, and the left tibiae were harvested and stored in 70% ethanol. To assess how bone's physical properties differ between adolescence (10 weeks of age) and young adulthood, four additional female Sprague-Dawley rats from the same breeding colony were killed at 5 months of age and weighed, and the left tibiae were harvested and stored as described above.

### Sample Preparation for Chemical and Mechanical Analysis

As a measure of growth, the length of the tibia was measured using digital calipers (Mitutoyo America, Aurora, IL, USA). Mid-lengths of all tibiae were marked and mid-diaphysal sections isolated by transversely transecting the bone 2 mm proximal and 5 mm distal to the mid-length mark (diamond wafer saw). Bone marrow was irrigated with distilled water, and samples were dehydrated in an increasing series of alcohol (70%, 80%, 90%, 100% ethanol). Samples were then embedded in low-viscosity epoxy resin (Epo-thin, Buehler, Lake bluff, IL, USA) under vacuum to allow for complete penetration of the epoxy into the marrow cavity. Using silicon carbide abrasive paper of decreasing particle size, the proximal surface of the embedded samples was sanded under deionized water until the mid-length mark was reached. To produce a glass-like smooth surface, the block was polished with diamond suspension (Metadi Supreme, Buehler, Lakebluff, IL, USA) using decreasing particle size from 3 to 1 to 0.2 to 0.05  $\mu\text{m}$ . Specimens were ultrasonically cleaned to remove surface debris and glued (cyanoacrylate) to steel microscope slides for infrared spectroscopy and nanoindentation testing. Spatial correlations between chemical and nanomechanical properties required the quantification of mechanical properties in precisely the same

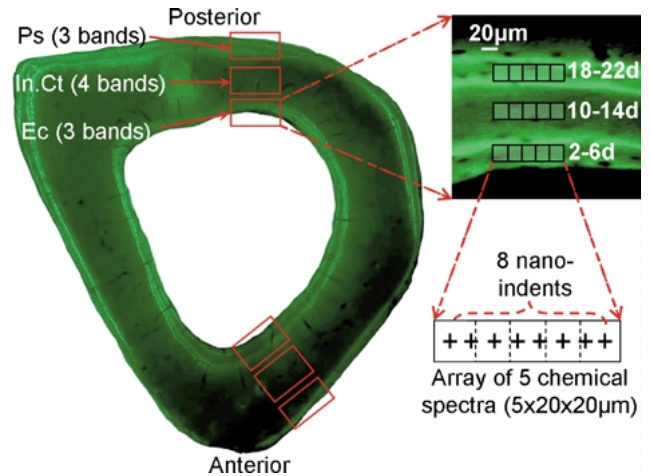


**Fig. 1.** Methodology used for collecting chemical and mechanical properties of bone with clearly defined age. Measurements were performed in 10 radial bands at the anterior as well as posterior cortices (*left panel*). Six of the bands were defined by fluorescent labels, three bands each at the endocortical region (*Ec, right panel*) and at the periosteal region (*Ps*) and four bands intracortically (*In.Ct*). The 10 and 14 days xylenol orange labels are not visible in this picture as they require a different filter for visualization. A  $100 \times 20 \mu\text{m}$  array was placed into each region (*right panel*) to collect five chemical spectra and eight nanoindentations. The arrays were contained between labels and were not in contact with them.

regions in which chemical properties were quantified. To this end, a two-dimensional coordinate system was defined by three reference points that were scratched into the surface of the epoxy block with a fine pin. This coordinate system was used for the electronic stages of both the infrared microscope and the nanoindenter. The precision and accuracy of the coordinate transformation were high, and the error in reproducing surface coordinates between the two systems did not exceed 5  $\mu\text{m}$ .

### Infrared Microspectroscopy

Synchrotron infrared microspectroscopy (SIRMS) allowed for the *in situ* analysis of collagen and mineral content and composition at spatial high resolution [26, 27]. Synchrotron light (National Synchrotron Light Source, Brookhaven National Laboratory, Upton, NY) was used as a light source for a Nicolet Magna 860 spectrometer (ThermoNicolet, Madison, WI) coupled to a Continuum IR microscope and MCT-A (HgCdTe photoconductive) detector using a frequency range of  $4,000\text{--}650 \text{ cm}^{-1}$ . A camera was mounted to the microscope to enable imaging of the specimens. A mercury arc lamp and wide band blue filter cube (WB-B; Olympus, Tokyo, Japan) allowed simultaneous visualization of the fluorescent labels in the bone matrix. Spectra were collected in reflectance mode, 128 scans per point, at  $4 \text{ cm}^{-1}$  spectral resolution using Omnic 6.1 software (ThermoNicolet), with the aperture size set at  $20 \times 20 \mu\text{m}$ . Decay of the current of the synchrotron light source was corrected for by multiplying each spectrum with a current correction factor to normalize all reflectance values. A Kramers-Kronig transformation converted the data from *percent reflectance* to *absorbance* units.

Measurements were taken from the anterior and posterior cortices of the mid-diaphysis, which was subdivided into 10 radially distinct bands. In the 10-week-old animals, six of the 10 bands were defined by the borders of any given double fluorescent label. Starting at either the endocortical or periosteal surface, these bands encompassed tissue that was either 2–6, 10–14, or 18–22 days old; and chemical spectra were measured

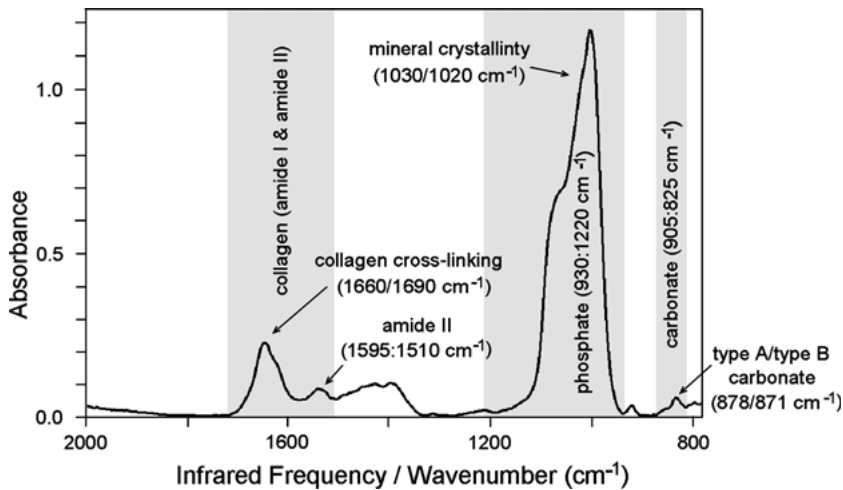


**Fig. 2.** Typical IR microspectrum obtained from the mid-diaphyseal tibia of a 10-week-old rat, illustrating the collagen, phosphate, and carbonate peaks.

in five adjacent  $20 \times 20 \mu\text{m}$  arrays that were centered in each of the six bands at both the anterior and posterior cortices (Fig. 1). The region between the two oldest (21 days) labels was defined as intracortical bone, which was further divided into four equidistant bands because of the large width of this region compared to the other six (surface) bands. Identical to the methodology used for the surface bands, chemical spectra were quantified in the center of each of the four intracortical bands via  $100 \times 20 \mu\text{m}$  arrays (Fig. 1). Thus, 100 chemical spectra were collected from tibial cortex of each 10-week-old rat, arising from five spectra within each of the 10 radial bands at both the anterior and posterior cortices. For the 5-month-old rats, chemical spectra were collected only intracortically within four bands as described for the 10-week-old rats. The spatial coordinates of each spectrum were recorded.

Chemical parameters were measured by calculating peak area and peak height of each spectrum (Fig. 2). The phosphate-to-protein ratio was calculated as the integrated area of the  $\nu_1\nu_3$  phosphate peak ( $1,220\text{--}930 \text{ cm}^{-1}$  with a baseline at  $1,220\text{--}930 \text{ cm}^{-1}$ ) to the amide II peak ( $1,595\text{--}1,510 \text{ cm}^{-1}$  with a linear baseline at  $1,800 \text{ cm}^{-1}$ ) [28]. The carbonate-to-protein ratio was determined by the integrated area of the carbonate peak at  $\nu_2$  ( $905\text{--}825 \text{ cm}^{-1}$  with a baseline at  $905\text{--}825 \text{ cm}^{-1}$ ) to the amide II peak. The ratio of type A carbonate ( $\text{OH}^-$  substitution) at  $878 \text{ cm}^{-1}$  to type B carbonate ( $\text{PO}_4^{3-}$  substitution) at  $871 \text{ cm}^{-1}$ , the phosphate-to-carbonate ratio, and mineral crystallinity ( $1,030/1,020 \text{ cm}^{-1}$  with a baseline at  $1,220\text{--}930 \text{ cm}^{-1}$ ) [30, 31] were also computed. These ratios may influence bone's mechanical properties through mineral substitutions into the hydroxyapatite lattice, which may alter crystal size, density, solubility, and surface defects [29–32]. A collagen cross-linking parameter, defined as the ratio of reducible to nonreducible cross-links, was calculated from the intensity ratio of amide I peaks at  $1,660$  and  $1,690 \text{ cm}^{-1}$ . Collagen cross-linking defines the quality and maturity of the fibers and contributes to the strength of collagen-mineral bonding [21]. Chemical parameters referred to above were calculated for each  $20 \times 20 \mu\text{m}$  square, and the median value of any given  $100 \times 20 \mu\text{m}$  array was used for further analysis.

### Nanoindentation

After IR spectral analyses, the mechanical material properties of the 10 distinct bands were assessed via nanoindentation (Tribolindenter; Hysitron, Minneapolis, MN, USA) at both the endocortical and periosteal surfaces. As described above, nanomechanical data points were collected in the same regions in which chemical data points were collected. The position of the coordinate reference points was selected with an optical microscope and a precision X-Y stage ( $500 \text{ nm}$  accuracy) attached to the nanoindenter. Within the same  $100 \times 20 \mu\text{m}$

arrays, eight indents were distributed evenly, with each indent  $10 \mu\text{m}$  apart (Fig. 1). Thus, 160 indents were made on each sample across the 10 bands at the anterior and posterior cortices. Indentations were performed using a trapezoidal waveform (10 seconds each of loading, holding, and unloading), with a peak load of  $1 \text{ mN}$  and loading rate of  $100 \mu\text{N}/\text{second}$  using a diamond Berkovich tip. Fused silica, which is elastically isotropic and has a relatively low modulus-to-hardness ratio, was used to calibrate the tip shape function and to check on the accuracy of the measurements. The optic-probe tip calibration was performed regularly to calibrate the offset between the probe tip and the optics focal point. The reduced elastic modulus ( $E_r$ ) was calculated by the standard Oliver-Pharr method [33],  $E_r = \frac{\sqrt{\pi}}{2} \frac{S}{\sqrt{A_c}}$ , where  $S$  is the contact stiffness and  $A_c$  is the contact area.  $E_r$  was used to determine the bone elastic modulus ( $E_b$ ), for each  $20 \times 20 \mu\text{m}$  square,  $E_b = \frac{1-\nu_b^2}{E_r - \frac{1-\nu_i^2}{E_i}}$ , where  $\nu$  is Poisson's ratio and the sub-

scripts  $b$  and  $i$  refer to bone and the indenter, respectively. The elastic properties of the diamond indenter were  $\nu_i = 0.07$  and  $E_i = 1,140 \text{ GPa}$ , and Poisson's ratio of bone was assumed to be  $0.3$ . In the following, only  $E_b$  is reported and referred to as  $E$ . In analogy to the chemical measurements, the median elastic modulus and hardness across each  $100 \times 20 \mu\text{m}$  array was used for further analysis.

### Statistical Analysis

One-way analysis of variance (ANOVA) followed by a Student-Neumann-Keul post-hoc test compared the chemical and nanoindentation parameters across the different radial band regions. Differences between the anterior and posterior cortices were assessed by paired two-tailed  $t$ -tests. Multiple linear regressions tested for associations between chemical and mechanical properties across the regions in which they were determined. Initially, 14 data points were entered into these correlations, representing averages across the eight 10-week-old rats for the six radial bands each at the anterior and posterior surface and one data point from each pooled intracortical region. Correlations were then expanded to 16 data points by adding the pooled intracortical regions of the four 5-month-old rats (i.e., the four intracortical arrays were pooled and averaged across the four rats, yielding one data point for the anterior cortex and one data point for the posterior cortex). Chemical and mechanical values that exceeded the mean  $\pm 2$  standard deviations (SDs) within an array of five (eight) data points, indicating tissue inhomogeneity (e.g., porosity) or high degree of surface roughness, were excluded from the array. Statistical tests were performed in SPSS (12.0; Chicago, IL), and statistical significance was set at  $5\%$ .

**Table 1.** Mean ratios ( $\pm$ SD) of phosphate-to-protein, carbonate-to-protein, crystallinity ( $1,030/1,020\text{ cm}^{-1}$ ), collagen cross-linking, type A to type B carbonate, and the elastic modulus (GPa) measured in regions of different age and pooled across anterior and posterior cortices

Age	Surface	Phosphate/protein	Carbonate/protein	$1,030/1,020\text{ cm}^{-1}$	Cross-linking	Type A/type B	Elastic modulus
2–6 days	Ec	$13.3 \pm 1.5^{a,b}$	$0.107 \pm 0.041^b$	$1.52 \pm 0.17$	$2.81 \pm 0.25$	$1.32 \pm 0.19$	$26.9 \pm 2.4$
	Ps	$13.7 \pm 1.2^{a,b}$	$0.112 \pm 0.030^b$	$1.60 \pm 0.30$	$2.74 \pm 0.32$	$1.38 \pm 0.31$	$26.1 \pm 2.7$
10–14 days	Ec	$15.2 \pm 2.3$	$0.122 \pm 0.024^b$	$1.67 \pm 0.45$	$2.93 \pm 0.49$	$1.38 \pm 0.18$	$27.7 \pm 1.9$
	Ps	$15.5 \pm 2.3$	$0.131 \pm 0.027^b$	$1.67 \pm 0.40$	$2.84 \pm 0.40$	$1.38 \pm 0.21$	$27.6 \pm 3.5$
18–22 days	Ec	$14.9 \pm 0.8$	$0.129 \pm 0.021^b$	$1.74 \pm 0.56$	$2.92 \pm 0.36$	$1.44 \pm 0.14$	$27.9 \pm 2.8$
	Ps	$15.7 \pm 2.7$	$0.131 \pm 0.024^b$	$1.65 \pm 0.36$	$2.94 \pm 0.34$	$1.50 \pm 0.20$	$28.3 \pm 3.9$
10 weeks	In.Ct	$17.0 \pm 2.5$	$0.134 \pm 0.018^b$	$1.67 \pm 0.36$	$3.06 \pm 0.42$	$1.53 \pm 0.10$	$28.4 \pm 3.0$
5 months	In.Ct	$17.0 \pm 1.8$	$0.174 \pm 0.024$	$1.77 \pm 0.08$	$2.99 \pm 0.27$	$1.53 \pm 0.14$	$28.8 \pm 2.6$

Ec, endocortical, Ps, periosteal, In.Ct, intracortical

<sup>a</sup> Significantly different from 10-week intracortical bone

<sup>b</sup> Significantly different from 5-month intracortical bone

## Results

### Chemical and Mechanical Properties

Both the anterior as well as the posterior cortex showed continuous labels at the endocortical and periosteal surfaces in seven out of the eight 10-week-old rats (Fig. 1). In one rat, labels were incomplete at the periosteal surface at the anterior and posterior cortices and were not included in the analysis (i.e.,  $n = 7$  for data from the periosteal surface). All fluorescent labels were at least  $25\ \mu$  apart, allowing the positioning of the  $100 \times 20\ \mu\text{m}$  arrays in between labels without making contact with them. Differences in any given chemical property between the four intracortical bands in both the 10- and 5-month-old rats were statistically not significant; therefore, the average of these four regions was pooled into one value representing intracortical bone.

Comparisons of chemical properties between the radial bands (defined by fluorescent labels) at the anterior and posterior cortices showed that bone of any given age had similar chemical properties at both cortices ( $P > 0.05$ ). Therefore, to reduce noise, values from both cortices were pooled for further analysis. The phosphate-to-protein ratio, an indicator of mineralization, showed an increasing trend with matrix age (Table 1, Fig. 3). Statistically, only the 2- to 6-day-old mineralized tissue was lower ( $P < 0.05$ ) in its phosphate-to-protein ratio compared to intracortical bone (19.9% at periosteal surface, 22.3% at endocortical surface). For the carbonate-to-protein ratio, phosphate-to-carbonate, type A/type B carbonate ratio, crystallinity, and collagen cross-linking ratio, there were similar trends with matrix age; but ANOVA indicated that there were no significant differences between any of the seven radial bands (Table 1, Fig. 3).

For any given chemical property pertaining to any given age, there was no significant difference between the band at the endocortical surface and the equivalent band at the periosteal surface; therefore, values for any

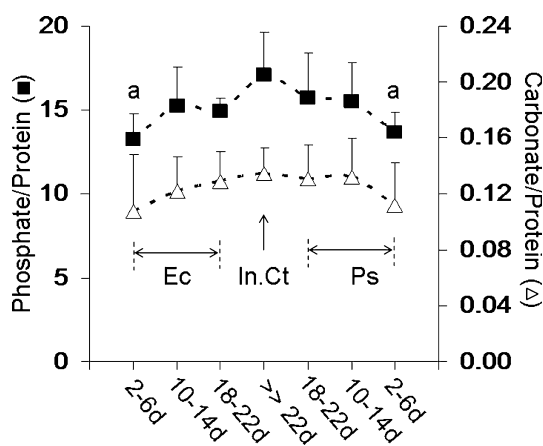


**Fig. 3.** Phosphate-to-protein ratio and carbonate-to-protein ratio quantified in seven radial bands between the endocortical (Ec) and periosteal (Ps) surfaces and averaged across the anterior and posterior cortices. The age of the tissue, as indicated by the presence of fluorescent labels, is given in days. *a*, Significant difference from intracortical region ( $>> 22$  days).

given age were pooled across the two surfaces for further analysis. Averaged across surfaces and cortices, the carbonate-to-protein ratio, crystallinity, type A/type B carbonate ratio, and collagen cross-linking all showed a similar age-related trend as the phosphate-to-protein ratio (described above); but differences between any of the regions did not reach statistical significance (Fig. 4). The magnitude of the elastic modulus that was determined in the same regions as the chemical properties increased with advancing age of the tissue, but statistically, no significant differences were detected between any of the regions when averaged across surfaces and cortices (Fig. 4).

### Comparison between 10-Week- and 5-Month-Old Rats

Five-month-old rats were included in the analysis to test for differences in bone's physical properties between an actively growing (10 weeks) and a young adult tibia.

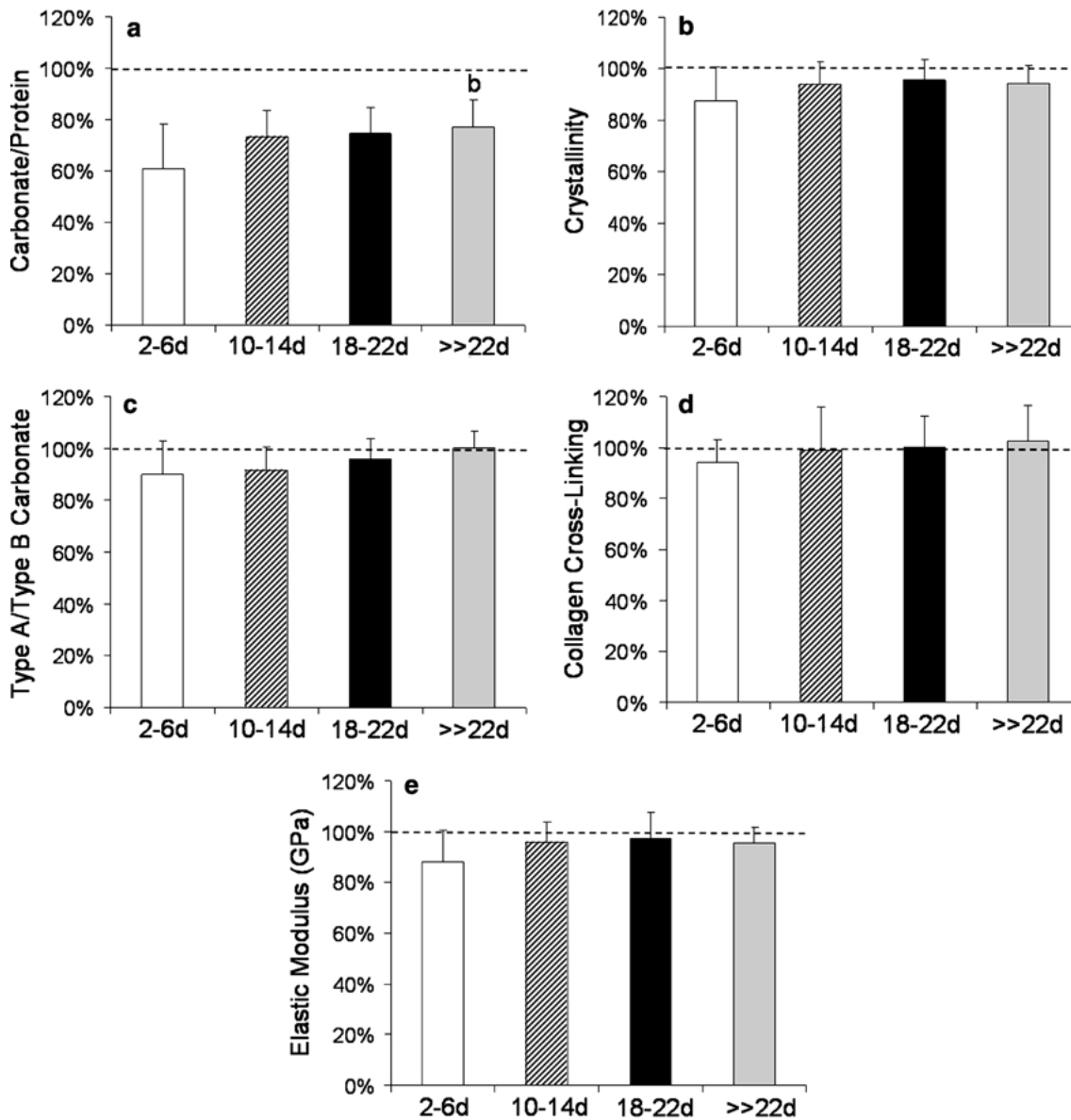


**Fig. 4.** Mean ( $\pm$ SD) (a) carbonate-to-protein ratio, (b) crystallinity ( $1,030/1,020\text{ cm}^{-1}$ ), (c) type A/type B carbonate ratio ( $878/871\text{ cm}^{-1}$ ), (d) collagen cross-linking ratio ( $1,660/1,690\text{ cm}^{-1}$ ), and (e) elastic modulus measured in the tibial diaphysis in which fluorescent labels indicated the age of the tissue. Tissue of any given age was averaged across the endocortical and periosteal surfaces of both the anterior and posterior cortices. Intracortical values of the tibial diaphysis from 5-month-old rats was used as a referent (dotted line), representing a value of 100%. *b*, Significant difference ( $P < 0.05$ ) between intracortical bone of 10-week- and 5-month-old rats.

Indicating a substantial difference in the level of maturity, the average body mass was 50% ( $P < 0.001$ ) greater in a 5-month-old rat than a 10-week-old rat ( $314 \pm 27$  vs.  $209 \pm 11$  g), while the length of the tibia was 16% ( $P < 0.001$ ) greater ( $41.3 \pm 0.7$  vs.  $35.7 \pm 0.3$  mm).

The phosphate-to-protein ratio was similar between the intracortical regions of 10-week- and 5-month-old rats ( $17.1 \pm 2.5$  vs.  $17.0 \pm 1.78$ ). Likewise, there were also no significant differences in the phosphate-to-carbonate, crystallinity, type A/type B carbonate ratio, and collagen cross-linking between the intracortical bone of 10-week- and 5-month-old rats (Table 1, Fig. 4). In contrast, the

intracortical carbonate-to-protein ratio of 10-week-old rats, averaged across the two cortices, was 23% smaller ( $P < 0.01$ ) than the intracortical value for 5-month-old rats (Fig. 4). The elastic mechanical properties of the tissue were similar between the intracortical regions of 10-week and 5-month-old rats (Table 1, Fig. 4).

#### *Correlation between Chemical and Mechanical Matrix Properties*

Sampled across the seven different radial bands at the anterior and posterior cortices ( $n = 14$ ), and averaged

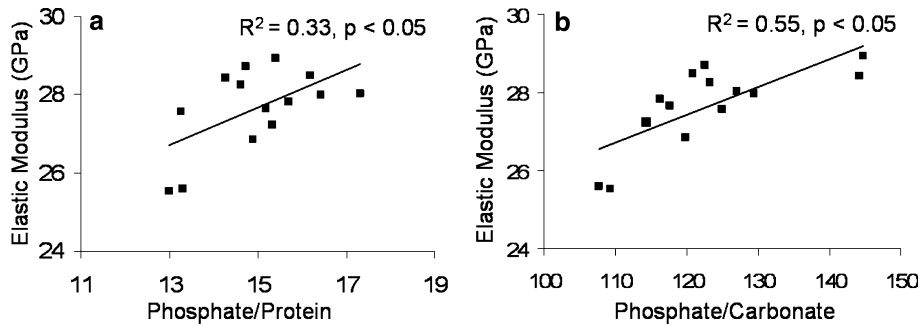


**Fig. 5.** Linear correlation between (a) the elastic modulus and the phosphate-to-protein ratio and (b) the elastic modulus and the phosphate-to-carbonate ratio collected from the 12 surface bands and two intracortical regions in 10-week-old rats.

across all 10-week-old rats, the phosphate-to-protein ratio was moderately correlated with the elastic tissue modulus ( $R^2 = 0.33$ ,  $P < 0.05$ ) (Fig. 5). The coefficient of determination improved to  $R^2 = 0.55$  ( $P < 0.01$ ) when phosphate was normalized to carbonate, rather than to protein. There were no significant relationships ( $R^2 < 0.1$ ,  $P > 0.5$ ) between the elastic modulus and the carbonate-to-protein ratio, crystallinity, type A/type B carbonate ratio, or collagen cross-linking ratio. Combining phosphate-to-protein and phosphate-to-carbonate in a multiple linear regression against the elastic modulus significantly increased the coefficient of determination ( $R^2 = 0.69$ ,  $P < 0.05$ ). Adding the remaining chemical ratios in the order of carbonate-to-protein, crystallinity, type A/type B carbonate, and collagen cross-linking to the multiple regression increased  $R^2$  from 0.69 to 0.78, 0.79, 0.80, and 0.83, respectively. The addition of the two intracortical data points from the 5-month-old rats rendered the correlation between the phosphate-to-carbonate ratio and the elastic modulus insignificant ( $R^2 = 0.15$ ,  $P > 0.05$ ), decreased the  $R^2$  value for the multiple regression involving all chemical ratios to 0.74 ( $P < 0.05$ ), but did not significantly alter the relation between the bone's stiffness and the phosphate-to-protein ratio ( $R^2 = 0.37$ ,  $P < 0.05$ ).

## Discussion

The hypothesis of this study was that primary and secondary mineralization of lamellar tissue formed during active growth of the skeleton would be slow because of the high demand, but limited availability, of mineral in the system. In contrast to this hypothesis, we found that, within a few days, lamellar bone formed during modeling in the rat tibia was able to establish many of its chemical and mechanical properties to a level that almost matched those of much older intracortical tissue. Spatial correlations across very small volumes of bone in which both chemical and mechanical properties were assessed revealed that a lower mechanical stiffness of the bone matrix was associated with a lower phosphate-to-carbonate ratio ( $R^2 = 0.55$ ) and, to a lesser extent, with lower phosphate-to-protein levels ( $R^2 = 0.33$ ). These data suggest that during surface modeling, large spatial

heterogeneities in chemical and mechanical properties across a bone can be avoided through exceedingly rapid mineralization of new tissue. Recognizing the importance of bone quality, this rapid attainment of bone mineral and stiffness may significantly contribute to the overall mechanical competence of bone as a structure [34].

Previous data suggested that the amount of mineral accumulated in the matrix during primary mineralization accounts for up to 50–70% of its peak properties and that secondary mineralization, at least in human osteonal bone, may take several years to complete [4–6]. In this study, primary mineralization accounted for up to 80% of mineralization levels reached at young adulthood (i.e., intracortical bone of 4-month-old rats) and the time required for secondary mineralization was less than 3 weeks. Of course, cellular metabolism is much higher in rats than in humans and may be related to faster mineralization times. In our study, rats were sexually mature but given the late cessation of longitudinal bone growth in this species [35, 36], skeletal maturity is often defined by a strong reduction in longitudinal and cross-sectional growth in bones of the appendicular skeleton, causing bone mass to approach a plateau. In female rats, this event occurs at approximately 12–15 weeks of age [37–39]. Thus, the 10-week-old rats in this study were considered actively growing while the 5-month-old rats were young adults, the large difference between the two groups reflected by a 50% difference in body mass. Considering that lamellar mechanical properties may plateau during young adulthood [24, 25], intracortical bone properties from the older group in this study may indicate an appropriate time point to estimate the end of secondary mineralization.

Chemical and mechanical properties were distributed relatively uniformly across cortices and surfaces within the mid-diaphysis, even though it is conceivable that tissue inhomogeneities were present at the two cortices that were not analyzed (medial and lateral). Nevertheless, our data are in contrast with studies that found differences in bone organic, inorganic, or mechanical properties between the anterior and posterior properties in a number of species [15, 38, 39]. They are, however,

entirely consistent with micromechanical studies that either were not able to detect significant differences in mechanical stiffness across a given diaphyseal cortex [40] or located only small differences in the elastic modulus across lamellae of different age during osteonal remodeling [41]. As differences in bone stiffness between opposing cortices may reflect differences in the locomotion-induced strain and stress environment (e.g., compression vs. tension) [42] and the mechanical milieu of the rat tibia has been characterized, due to its small size, only at specific anatomical locations of the mid-diaphysis [43], it is possible that the specific mechanical parameter(s) influencing mineralization is of similar magnitude at both the anterior and posterior cortices of the immature rat tibia. Alternatively, the effects of the nonuniform strain environment may have been masked by tight genetic control of bone formation and mineralization [44].

The complexity by which chemical and mechanical parameters define bone quality is reflected by the conflicting nature of many studies; while a number of chemical properties, including measures of mineral quantity [11–13, 15, 16], mineral quality [15, 16], or organic matrix quantity and quality [21, 22, 45], have been related to variations in bone's mechanical behavior, other data have been more equivocal [14, 18, 46, 47]. Aside from the different techniques used to probe chemical (e.g., Raman spectroscopy, IR spectroscopy, electron microscopy) and mechanical (e.g., whole-bone bending tests, nanoindentation, acoustic microscopy) properties, many discrepancies between these studies may lie in the different hierarchical levels [23] at which these relations were developed (i.e., organ vs. tissue vs. material). Almost all of the studies cited above relied on correlating differences in bone's physical properties that were caused by differences in age and physiological or pathological status of the individual. Our study is unique in the sense that nanoindentation and SIRMS coupled to an epifluorescence microscope allowed us to test for mechanochemical relations across spatial volumes of known age in individuals without potential confounding variables such as age or disease. Further, the microscopic level ( $<20\ \mu\text{m}$ ) at which all measurements were performed did not require consideration of voids and geometrical inhomogeneities that may have a substantial influence if data are collected at a more macroscopic level [48].

The few studies that have attempted such *in situ* correlations at the level of the material have reported equivocal results, ranging from poor [46] to moderate [12] correlations between mechanical and chemical properties, in essence framing data from this study in which 35% of the variation in Young's modulus was accounted for by bone's phosphate-to-protein ratio. Because of the very small variability in collagen cross-linking and the type A to type B carbonate ratio between

the different time points, neither parameter contributed to intrinsic stiffness. The substantial improvement in correlative strength when phosphate was normalized to carbonate content, rather than protein content, was unexpected, in particular because carbonate content itself was a very poor predictor of material stiffness. The phosphate-to-carbonate ratio reflects the degree of type A and type B carbonate substitution into locations of hydroxyl and phosphate ions of the mineral crystals, respectively [17, 49]. The substitution of carbonate ions for  $\text{OH}^-$  and  $\text{PO}_4^{3-}$  ions creates vacancies and distortion that may change the shape of the crystal lattice and affect the mechanical strength of a mineral crystal because of alterations in their local strain environment [17, 50]. While this may indicate that the ratio of phosphate to carbonate associated with a given volume of protein accounts for half of bone's stiffness, it is critical to point out that phosphate is the principal determinant of this relationship. In fact, carbonate levels of the different regions in tibial sections of 10-week-old rats (in which the correlations presented in this study were produced) were in a narrow range, and inclusion of data points from 5-month-old rats (in which carbonate levels were significantly greater) rendered the relation between phosphate-to-carbonate ratio and the elastic modulus insignificant, while the  $R^2$  value correlating the phosphate-to-protein ratio with the elastic modulus remained unchanged.

In conclusion, primary and secondary mineralization of lamellar bone may occur exceptionally rapidly during surface modeling. Microstructural techniques allowed for the characterization of several chemical and mechanical properties of any given volume of bone, and correlations across anatomical locations indicated that the combination of all considered chemical parameters was capable of explaining 80% of the variation in the elastic modulus. These *in situ* techniques also emphasized that the physical properties of bone that is a few days old in an adolescent skeleton could be at least an order of magnitude greater than those of a skeleton that is a few days old [51, 52]. Whether results from this study can be extrapolated to remodeling events induced by endogenous (e.g., hormonal) or exogenous (e.g., mechanical loading) stimuli in the human adult skeleton remains to be determined, but it is clear that a better understanding of functional relationships between chemical and mechanical components, in particular when combined with a rigorous appreciation of the underlying molecular and cellular events, may, in the future, lead to effective prophylaxes and treatments of reduced bone strength during aging or bone diseases.

*Acknowledgment.* Funding from NASA NAG 9-1499 (S.J.), the Whitaker Foundation RG-02-0564 (S.J.), NSBRI TD00207 (Y-XQ), and SUNY-BNL Seed (S.J.) was greatly appreciated. We also thank Ben Adler, Randy Smith, Liqin

Xie, and Dr. Erik Mittra for expert technical advice. Use of the National Synchrotron Light Source, Brookhaven National Laboratory, was supported by the U.S. Department of Energy, Office of Science, Office of Basic Energy Sciences, under contract DE-AC02 98CH10886.

## References

- Ehrlich PJ, Lanyon LE (2002) Mechanical strain and bone cell function: a review. *Osteoporos Int* 13:688–700
- Karsenty G (2003) The complexities of skeletal biology. *Nature* 423:316–318
- Seeman E (2002) Pathogenesis of bone fragility in women and men. *Lancet* 359:1841–1850
- Amprino R, Engstrom A (1952) Studies on X-ray absorption and diffraction of bone tissue. *Acta Anat (Basel)* 15:1–22
- Boivin G, Meunier PJ (2003) The mineralization of bone tissue: a forgotten dimension in osteoporosis research. *Osteoporos Int* 14(suppl 3):S19–S24
- Grynopas M (1993) Age and disease-related changes in the mineral of bone. *Calcif Tissue Int* 53(suppl 1):S57–S64
- Borah B, Ritman EL, Dufresne TE, Jorgensen SM, Liu S, Sacha J, Phipps RJ, Turner RT (2005) The effect of risedronate on bone mineralization as measured by micro-computed tomography with synchrotron radiation: correlation to histomorphometric indices of turnover. *Bone* 37:1–9
- van der Meulen MC, Jepsen KJ, Mikic B (2001) Understanding bone strength: size isn't everything. *Bone* 29:101–104
- Judex S, Boyd SK, Qin YX, Miller L, Muller R, Rubin CT (2003) Combining high-resolution microCT with material composition to define the quality of bone tissue. *Curr Osteoporosis Rep* 1:11–19
- Paschalis EP, Shane E, Lyritis G, Skarantavos G, Mendelsohn R, Boskey AL (2004) Bone fragility and collagen cross-links. *J Bone Miner Res* 19:2000–2004
- Ding M, Dalstra M, Danielsen CC, Kabel J, Hvid I, Linde F (1997) Age variations in the properties of human tibial trabecular bone. *J Bone Joint Surg Br* 79:995–1002
- Ferguson VL, Bushby AJ, Boyde A (2003) Nanomechanical properties and mineral concentration in articular calcified cartilage and subchondral bone. *J Anat* 203:191–202
- Follet H, Boivin G, Rumelhart C, Meunier PJ (2004) The degree of mineralization is a determinant of bone strength: a study on human calcanei. *Bone* 34:783–789
- McCalden RW, McGeough JA, Barker MB, Court-Brown CM (1993) Age-related changes in the tensile properties of cortical bone. The relative importance of changes in porosity, mineralization, and microstructure. *J Bone Joint Surg Am* 75:1193–1205
- Akkus O, Adar F, Schaffler MB (2004) Age-related changes in physicochemical properties of mineral crystals are related to impaired mechanical function of cortical bone. *Bone* 34:443–453
- Silva MJ, Ulrich SR (2000) In vitro sodium fluoride exposure decreases torsional and bending strength and increases ductility of mouse femora. *J Biomech* 33:231–234
- Penel G, Leroy G, Rey C, Bres E (1998) MicroRaman spectral study of the PO<sub>4</sub> and CO<sub>3</sub> vibrational modes in synthetic and biological apatites. *Calcif Tissue Int* 63:475–481
- Bailey AJ, Sims TJ, Ebbesen EN, Mansell JP, Thomsen JS, Mosekilde L (1999) Age-related changes in the biochemical properties of human cancellous bone collagen: relationship to bone strength. *Calcif Tissue Int* 65:203–210
- Oxlund H, Mosekilde L, Ortoft G (1996) Reduced concentration of collagen reducible cross links in human trabecular bone with respect to age and osteoporosis. *Bone* 19:479–484
- Rho JY, Roy ME, Tsui TY, Pharr GM (1999) Elastic properties of microstructural components of human bone tissue as measured by nanoindentation. *J Biomed Mater Res* 45:48–54
- Sims TJ, Miles CA, Bailey AJ, Camacho NP (2003) Properties of collagen in OIM mouse tissues. *Connect Tissue Res* 44(suppl 1):202–205
- Wang X, Bank RA, TeKoppele JM, Agrawal CM (2001) The role of collagen in determining bone mechanical properties. *J Orthop Res* 19:1021–1026
- Weiner S, Traub W (1992) Bone structure: from angstroms to microns. *FASEB J* 6:879–885
- Ferguson VL, Ayers RA, Bateman TA, Simske SJ (2003) Bone development and age-related bone loss in male C57BL/6J mice. *Bone* 33:387–398
- Somerville JM, Aspden RM, Armour KE, Armour KJ, Reid DM (2004) Growth of C57BL/6 mice and the material and mechanical properties of cortical bone from the tibia. *Calcif Tissue Int* 74:469–475
- Miller LM, Carlson CS, Carr GL, Chance MR (1998) A method for examining the chemical basis for bone disease: synchrotron infrared microspectroscopy. *Cell Mol Biol (Noisy-le-grand)* 44:117–127
- Miller LM, Novatt JT, Hamerman D, Carlson CS (2004) Alterations in mineral composition observed in osteoarthritic joints of cynomolgus monkeys. *Bone* 35:498–506
- Rey C, Shimizu M, Collins B, Glimcher MJ (1991) Resolution-enhanced Fourier transform infrared spectroscopy study of the environment of phosphate ion in the early deposits of a solid phase of calcium phosphate in bone and enamel and their evolution with age: 2. Investigations in the nu<sub>3</sub>PO<sub>4</sub> domain. *Calcif Tissue Int* 49:383–388
- Gadaleta SJ, Paschalis EP, Betts F, Mendelsohn R, Boskey AL (1996) Fourier transform infrared spectroscopy of the solution-mediated conversion of amorphous calcium phosphate to hydroxyapatite: new correlations between X-ray diffraction and infrared data. *Calcif Tissue Int* 58:9–16
- Paschalis EP, DiCarlo E, Betts F, Sherman P, Mendelsohn R, Boskey AL (1996) FTIR microspectroscopic analysis of human osteonal bone. *Calcif Tissue Int* 59:480–487
- Camacho NP, Hou L, Toledano TR, Ilg WA, Brayton CF, Raggio CL, Root L, Boskey AL (1999) The material basis for reduced mechanical properties in oim mice bones. *J Bone Miner Res* 14:264–272
- Gadaleta SJ, Boskey AL, Paschalis E, Carlson C, Menschik F, Baldini T, Peterson M, Rinnac CM (2000) A physical, chemical, and mechanical study of lumbar vertebrae from normal, ovariectomized, and nandrolone decanoate-treated cynomolgus monkeys (*Macaca fascicularis*). *Bone* 27:541–550
- Oliver WC, Pharr GM (1992) An improved technique for determining hardness and elastic modulus using load and displacement sensing indentation experiments. *J Mater Res* 7:1564–1583
- Van Der Linden JC, Birkenhager-Frenkel DH, Verhaar JA, Weinans H (2001) Trabecular bone's mechanical properties are affected by its non-uniform mineral distribution. *J Biomech* 34:1573–1580
- Martin EA, Ritman EL, Turner RT (2003) Time course of epiphyseal growth plate fusion in rat tibiae. *Bone* 32:261–267
- Danielsen CC, Mosekilde L, Svenstrup B (1993) Cortical bone mass, composition, and mechanical properties in female rats in relation to age, long-term ovariectomy, and estrogen substitution. *Calcif Tissue Int* 52:26–33
- Hunziker EB, Schenk RK (1989) Physiological mechanisms adopted by chondrocytes in regulating longitudinal bone growth in rats. *J Physiol* 414:55–71
- Fukuda S, Iida H (2004) Age-related changes in bone mineral density, cross-sectional area and the strength of long bones in the hind limbs and first lumbar vertebra in female Wistar rats. *J Vet Med Sci* 66:755–760

39. Li XQ, Klein L (1990) Age-related inequality between rates of formation and resorption in various whole bones of rats. *Proc Soc Exp Biol Med* 195:350–355
40. Rho JY, Zioupos P, Currey JD, Pharr GM (2002) Microstructural elasticity and regional heterogeneity in human femoral bone of various ages examined by nanoindentation. *J Biomech* 35:189–198
41. Rho JY, Zioupos P, Currey JD, Pharr GM (1999) Variations in the individual thick lamellar properties within osteons by nanoindentation. *Bone* 25:295–300
42. Goodwin KJ, Sharkey NA (2002) Material properties of interstitial lamellae reflect local strain environments. *J Orthop Res* 20:600–606
43. Keller TS, Spengler DM (1989) Regulation of bone stress and strain in the immature and mature rat femur. *J Biomech* 22:1115–1127
44. Judex S, Donahue LR, Rubin C (2002) Genetic predisposition to low bone mass is paralleled by an enhanced sensitivity to signals anabolic to the skeleton. *FASEB J* 16:1280–1282
45. Weiner S, Traub W, Wagner HD (1999) Lamellar bone: structure-function relations. *J Struct Biol* 126:241–255
46. Coats AM, Zioupos P, Aspden RM (2003) Material properties of subchondral bone from patients with osteoporosis or osteoarthritis by microindentation testing and electron probe microanalysis. *Calcif Tissue Int* 73: 66–71
47. Zioupos P, Currey JD, Hamer AJ (1999) The role of collagen in the declining mechanical properties of aging human cortical bone. *J Biomed Mater Res* 45: 108–116
48. Silva MJ, Brodt MD, Fan Z, Rho JY (2004) Nanoindentation and whole-bone bending estimates of material properties in bones from the senescence accelerated mouse SAMP6. *J Biomech* 37:1639–1646
49. Frushour BG, Koenig JL (1975) Raman scattering of collagen, gelatin, and elastin. *Biopolymers* 14:379–391
50. Baig AA, Fox JL, Young RA, Wang Z, Hsu J, Higuchi WI, Chhetry A, Zhuang H, Otsuka M (1999) Relationships among carbonated apatite solubility, crystallite size, and microstrain parameters. *Calcif Tissue Int* 64: 437–449
51. Tanck E, Donkelaar CC Van, Jepsen KJ, Goldstein SA, Weinans H, Burger EH, Huiskes R (2004) The mechanical consequences of mineralization in embryonic bone. *Bone* 35:186–190
52. Tarnowski CP, Ignelzi MA J., Morris MD (2002) Mineralization of developing mouse calvaria as revealed by Raman microspectroscopy. *J Bone Miner Res* 17: 1118–1126